Emergence of Superconductivity, Valence Bond Order, and Mott Insulators in Pd[(dmit)$_2$] Based Organic Salts

Jeffrey G. Rau[1] and Hae-Young Kee[1,2,*]

[1]Department of Physics, University of Toronto, Toronto, Ontario M5S 1A7, Canada
[2]Canadian Institute for Advanced Research/Quantum Materials Program, Toronto, Ontario M5G 1Z8, Canada

(Received 1 August 2010; published 4 February 2011)

The $EtMe_3P$ and $EtMe_3Sb$ triangular organic salts are distinguished from other Pd[(dmit)$_2$] based salts, as they display valence bond and no long-range order, respectively. Under pressure, a superconducting phase is revealed in $EtMe_3P$ near the boundary of valence bond order. We use slave-rotor theory with an enlarged unit cell to study competition between uniform and broken translational symmetry states, offering a theoretical framework capturing the superconducting, valence bond order, spin liquid, and metallic phases on an isotropic triangular lattice. Our finite temperature phase diagram manifests a remarkable resemblance to the phase diagram of the $EtMe_3P$ salt, where the reentrant transition of insulator-metal-insulator type can be explained by an entropy difference between the metal and U(1) spin liquid. We predict different temperature dependence of the specific heat between the spin liquid and metal.

DOI: 10.1103/PhysRevLett.106.056405 PACS numbers: 71.27.+a

Quasi-two-dimensional organic salts have provided a playground to study the rich physics of frustrated and strongly correlated systems. One fascinating example is the family of triangular $Z[Pd(dmit)_2]_2$ salts where Z is a monovalent cation and dmit refers to 1,3-dithiol-2-thione-4,5-dithiolate. At ambient pressure, most $[Pd(dmit)_2]_2$ compounds are paramagnetic Mott insulators with spin susceptibility showing the characteristic temperature dependence of a spin-1/2 Heisenberg antiferromagnet at high temperatures [1]. If geometrical frustration is less effective, one expects long-range order to develop at low temperatures to release the spin entropy. Antiferromagnetic (AFM) order is a natural candidate, which is indeed observed in the cases of $Z = Me_4P$, Me_4Sb, Me_4As, Et_2Me_2P, and Et_2Me_2As [1]. However, no long-range order has been detected in $EtMe_3Sb$ [2–4], potentially exhibiting a spin liquid (SL) phase, and in $EtMe_3P$ [5,6] a spin-gapped phase with columnar valence bond (VB) order emerges.

While most $[Pd(dmit)_2]_2$ salts become metallic [6] under pressure, the $EtMe_3P$ salt exhibits superconductivity with maximum T_c appearing at the border of the VB phase seen in x-ray measurements [5,6]. Reentrant transitions of the form insulator-metal-insulator near the phase boundary at low temperatures were reported [6], where the positive curvature of the phase boundary indicates a large entropy contained in the paramagnetic insulator relative to the metallic phase. The complexity presented in the phase diagram of $EtMe_3P$ has not yet been explained within a single theoretical framework.

In this Letter, we provide a microscopic theory which demonstrates the emergence of the superconducting, VB ordered, SL, and metallic phases. We focus on an isotropic triangular lattice aiming to understand the phenomena observed in the $EtMe_3P$ and $EtMe_3Sb$ salts. In addition to the well-known on-site Hubbard interaction, we find that a spin-spin interaction plays an essential role in favoring the different ground states reported for $EtMe_3P$ and $EtMe_3Sb$. Our theory also provides a SL surviving between the metal and VB ordered phases, superconducting pairing symmetry, and novel behavior of the specific heat across the metal-insulator transition.

A common theoretical approach for Mott insulators is to start from a localized Heisenberg spin model. However, $EtMe_3P$ becomes metallic or superconducting when pressure is applied, exhibiting a metal-insulator (MI) transition. Capturing the MI transition requires an electronic description, such as a Hubbard model at an intermediate coupling [7–12]. Can one access the competition between SL and VB ordered insulators and between metal and superconductor within the Hubbard model near the MI transition? Prior work [13,14] suggests difficulty in achieving a superconducting phase within the pure Hubbard model at intermediate coupling in contrast to when a spin-spin interaction is included. Combining the experimental facts and the previous theoretical work, we suggest the following t-U-J Hamiltonian is a minimal model for isotropic triangular $[Pd(dmit)_2]_2$ salts:

$$H = -t\sum_{\langle ij\rangle\sigma} c^\dagger_{i\sigma}c_{j\sigma} + U\sum_i n_{i\uparrow}n_{i\downarrow} + J\sum_{\langle ij\rangle}\vec{S}_i\cdot\vec{S}_j, \quad (1)$$

where $\sum_{\langle ij\rangle}$ runs over nearest neighbors, $t > 0$ is the nearest neighbor hopping (we will set $t = 1$ as our energy scale below), U is the on-site Hubbard repulsion, and J is the spin-spin interaction. We emphasize that the J term is being considered as an independent effective interaction. The $c_{i\sigma}$ and $c^\dagger_{i\sigma}$ are the electron operators, and the electron spin operator is $\vec{S}_i = \sum_{\alpha\beta}c^\dagger_{i\alpha}(\vec{\sigma})_{\alpha\beta}c_{i\beta}$, where $\vec{\sigma}$ are the Pauli matrices. In this model our sites are pairs of molecules and thus U and J are effective interactions for the whole molecular dimer.

We take a slave-rotor approach [15] which can handle the intermediate coupling regime where charge fluctuations are important. In the slave-rotor representation [15], the electron operators are expressed as $c_{i\sigma} = f_{i\sigma} e^{i\theta_i}$, where $\exp(-i\theta_i)$ is the rotor lowering operator and $f_{i\sigma}$, $f^\dagger_{i\sigma}$ are fermionic spinon operators. Using this representation the Hamiltonian (1) is written as [15]

$$H = -t\sum_{\langle ij\rangle\sigma} f^\dagger_{i\sigma} f_{j\sigma} e^{-i(\theta_i-\theta_j)} + \frac{U}{2}\sum_i L_i(L_i-1) + J\sum_{\langle ij\rangle} \vec{S}^f_i \cdot \vec{S}^f_j,$$

where $\vec{S}^f_i = 1/2\sum_{\alpha\beta} f^\dagger_{i\alpha}(\vec{\sigma})_{\alpha\beta} f_{i\beta}$ is the spinon spin operator and L_i is the rotor charge operator [15]. It is important that the constraint of $L_i + \sum_\alpha f^\dagger_{i\alpha} f_{i\alpha} = 1$ be satisfied to project the Hilbert space into the physical subspace at half filling.

We adopt the slave-rotor theory and extend to an enlarged, two site unit cell to study the competition between uniform states and states which minimally break physical translational invariance. The spinon operators for the two sites in our unit cell are denoted by $c_{i\sigma}$ and $d_{i,\sigma}$ as indicated in Fig. 1. Introducing the mean fields, $\chi_{ij} = \frac{1}{2}\sum_\sigma \langle f^\dagger_{i\sigma} f_{j\sigma}\rangle$, $B_{ij} = \langle e^{-i(\theta_i-\theta_j)}\rangle$, and $\Delta_{ij} = \langle f^\dagger_{i\uparrow} f^\dagger_{j\downarrow}\rangle$, the spinon part of the Hamiltonian is given by

$$\begin{aligned} H_f &= -\sum_{\sigma\langle ij\rangle}\left(tB_{ij} + \frac{3J}{2}\chi^*_{ij}\right) f^\dagger_{i\sigma} f_{j\sigma} - \frac{3J}{8}\sum_{\langle ij\rangle}[\Delta_{ij}(f_{i\downarrow} f_{j\uparrow} \\ &\quad - f_{i\uparrow} f_{j\downarrow}) + \text{H.c.}] + \sum_{ij}\left(\frac{3J}{2}|\chi_{ij}|^2 + \frac{3J}{8}|\Delta_{ij}|^2\right) \\ &\equiv \sum_{\mathbf{k}} \Psi^\dagger_{\mathbf{k}} M_{\mathbf{k}} \Psi_{\mathbf{k}} + N\sum_{r=1}^{6}\left(\frac{3J}{2}|\chi_r|^2 + \frac{3J}{8}|\Delta_r|^2\right) + E_0, \end{aligned}$$

where $M_{\mathbf{k}}$ is 4×4 matrix in the basis of $\Psi_{\mathbf{k}} = (c^\dagger_{\mathbf{k}\uparrow}, d^\dagger_{\mathbf{k}\uparrow} c_{-\mathbf{k}\downarrow}, d_{-\mathbf{k}\downarrow})$ reflecting the unit cell doubling in particle-hole Nambu basis. The additive constant is the Fermi sea energy.

Treating the rotors as a bosonic variable, i.e., $e^{i\theta_i} = \phi_i$ subject to the constraint of $|\phi_i|^2 = 1$, the rotor part of the Hamiltonian can be represented by the (imaginary time) action,

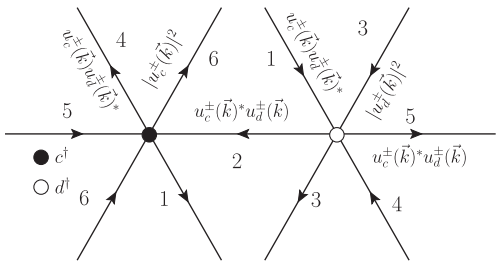

FIG. 1. The doubled unit cell and form factors $g^\pm_r(\vec{k})$.

$$\begin{aligned} S &= \int_0^\beta d\tau\left[\sum_i\left(\frac{|\partial_\tau\phi_i|^2}{2U} + i\lambda_i|\phi_i|^2\right) - 2t\sum_{\langle ij\rangle}\chi_{ij}\bar{\phi}_i\phi_j\right] \\ &\equiv \sum_{k\omega}[\gamma^+_k|\zeta_+(\vec{k},\omega)|^2 + \gamma^-_k|\zeta_-(\vec{k},\omega)|^2], \end{aligned}$$

where the final form is obtained as in the spinon case by decomposing into the two sublattices and Fourier transforming. The $i\lambda_i (\equiv h)$ enforces the constraint and acts as a chemical potential. To consider condensation, we separate out the lowest energy component of the lower band γ^-_k by diagonalizing the above action and assuming $\vec{k} = 0$ condensation can be treated as an independent variable. Denoting the condensate density as $|z|^2$, the saddle point conditions for h_a, h_b, and z give constraint equations for the number of bosons.

The full set of mean-field equations is given as

$$\begin{aligned} \chi_r &= \frac{1}{N}\sum_k\sum_{l=1}^4 n_f(E_l(\vec{k}))[U^\dagger_k O_{\chi_r}(\vec{k}) U_k]_{ll}, \\ \Delta_r &= \frac{1}{N}\sum_k\sum_{l=1}^4 n_f(E_l(\vec{k}))[U^\dagger_k O_{\Delta_r}(\vec{k}) U_k]_{ll}, \\ B_r &= \frac{1}{N}\sum_{k\alpha} e^{i\vec{k}\cdot\hat{\delta}_r} g^\alpha_r(k) n_b(\gamma^\alpha_k) + g^-_r(0)|z|^2, \end{aligned} \tag{2}$$

where $\alpha = \pm$, the $g^\alpha_r(k)$ form factors with $r = 1$–6 are defined in Fig. 1, $E_l(\vec{k})$ are the eigenvalues of M_k, and U_k is the matrix of eigenvectors. The 4×4 matrices $O_X(\vec{k})$ are defined by the schematic relation $X = \frac{1}{N}\sum_k \langle \Psi^\dagger_k O_X(\vec{k}) \Psi_k\rangle$. The bosonic distribution $n_b(x)$ is defined as $n_b(x) = \sqrt{U/2x}\coth(\beta\sqrt{Ux/2})$ and $n_f(x)$ is the Fermi function. The constraint equations for the number of fermions and bosons are given by

$$\begin{aligned} &\frac{1}{N}\sum_k\sum_{l=1}^4 n_f(E_l(\vec{k}))[U^\dagger_k O_{n_s}(\vec{k}) U_k]_{ll} = 1, \\ &|u^-_s(0)|^2|z|^2 + \frac{1}{N}\sum_{k\neq 0,\alpha}|u^\alpha_s(\vec{k})|^2 n_b(\gamma^\alpha_k) = 1, \end{aligned} \tag{3}$$

where $s = c, d$, the form factors $u^\pm_s(\vec{k})$ are the components of the rows of the transformation matrix that takes the rotor action to diagonal form, and n_c, n_d are the densities on each sublattice. When the condensation amplitude is finite we also have $\gamma^-_0|z| = 0$.

Figure 2 shows zero-temperature phase diagram varying J and U obtained by solving the above coupled mean-field equations of Eq. (2) self-consistently while enforcing the constraints of Eq. (3). This involves 12 complex mean fields, 6 χ_{ij} and 6 B_{ij} as indicated in Fig. 1, linking the fermionic and bosonic mean-field theories of the spinon and rotor sectors, respectively. For the pairing we use an ansatz of $\Delta_r = |\Delta| e^{i\theta_{\delta_r}}$ with uniform magnitude but allow the phase to vary within the unit cell.

Four phases are identified in Fig. 2: a superconductor, a metal, a SL, and the dimer state. The uniform metallic state

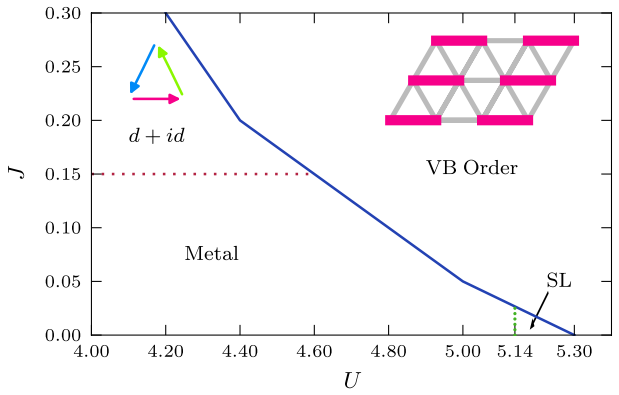

FIG. 2 (color online). The J vs U phase diagram. The dotted line denotes a second-order transition, while the solid line is first-order. The label $d + id$ denotes the superconducting phase, and the inset shows the phase of Δ on each bond. The U(1) spin liquid is labeled SL. The pattern of χ and B in the VB ordered state is inset in the VB phase, with thick lines denoting large values and thin lines small values. We have rescaled $U \to U/2$ as discussed in [15].

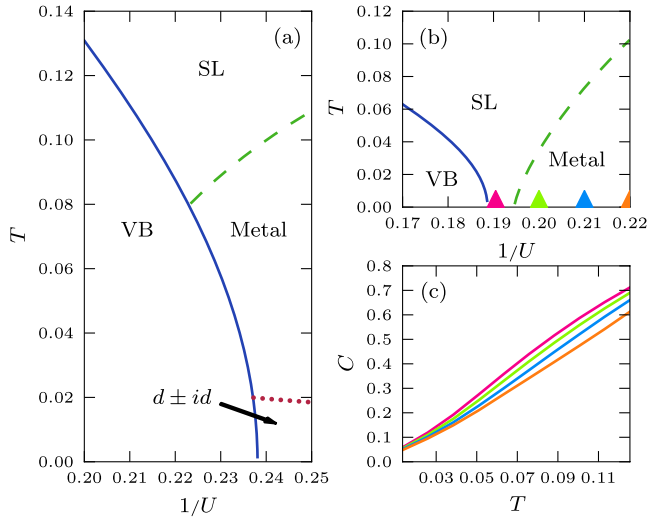

FIG. 3 (color online). Finite temperature phase diagrams, with $J = 0.25$ for (a) and $J = 0.00$ for (b). Curves have been fitted to the boundaries to guide the eye. A dotted line denotes a second-order transition, a solid line is first-order transition, and a dashed line is a crossover. Note the superconducting phase at small U for $J = 0.25$ in (a). In (c) specific heat as a function of T is shown for various values of U denoted by different colors in (b). Note that the slope of the curves increases with U indicating more density of states in SL insulator than metal.

is characterized by the condensation of the bosonic degree of freedom and a uniform, real $\chi_{ij} = |\chi|$ implying the existence of an electron Fermi surface and gapless charge excitations. On the insulating side, the SL is also characterized by a uniform, real χ_{ij} but gapped bosons, meaning the existence of a spinon Fermi surface but gapped charge excitations. The dimerized phase is characterized by $\chi_2 = 1/2$ and remaining $\chi_i = 0$ (with a similar structure for B) and $\Delta = 0$. Since the mean-field solution consists of completely isolated bonds, any dimer covering of the triangular lattice has the same mean-field energy at this level of approximation. In the superconductor we find the pairing is $d \pm id$ [16,17], as the phase winds by $2\pi/3$ around a triangle. It is fully gapped, with no nodes. Note that we do not find a $\mathbb{Z}_2$ SL, that is a SL phase with finite spinon pairing but uncondensed rotor bosons.

One can show via perturbation theory that if $U/t \gg 1$, $B_{ij} \sim 4t\chi^*_{ij}/U$, so the spinon Hamiltonian becomes identical to a slave-fermion description of the Heisenberg model with $J = 4t^2/U$. The result of Rokhsar [18] states that under our conditions a dimerized configuration is among the mean-field ground states. Thus we expect a dimerized state at large U. However, the U(1) SL survives between the metal and VB ordered phases near MI transition due to charge fluctuations. The window of spin liquid phase is quickly wiped out as we increase J. One expects that as J becomes large our mean-field solution will be equivalent to that of a Heisenberg model decoupled in χ and Δ channels. The argument of Rokhsar [18] can be generalized to this case, and implies that the mean-field ground states include dimerized states, where $\chi_{ij} = \Delta_{ij} = 0$ on some bonds while on others $|\chi_{ij}|^2 + |\Delta_{ij}|^2$ is maximal. Thus we expect that the dimerized state will be among the ground states as we increase J. Lee and Lee [19] have looked at the pure Hubbard model ($J = 0$) considering only translationally invariant solutions, and found a continuous transition from a metal into a SL. One may speculate that the SL is wiped out by some translationally broken symmetry state, but we find that a window of SL still survives between the metal and VB ordered phase.

It is straightforward to compute finite temperature phase diagrams as shown in Figs. 3(a) and 3(b). One peculiarity is that there is no condensation of the bosons in two dimensions at any finite temperature, and thus no metallic phase. This is an artifact of the spherical approximation, that is treating the rotors as bosons [15]. As the rotor action is equivalent to one used to describe Josephson junction arrays, we expect a Kosterlitz-Thouless-type transition from metal to SL, with quasi-long-range order at low temperatures. In fact, including gauge fluctuations, the nature of the phase transition from metal to SL may be a crossover [20,21]. In Figs. 3(a) and 3(b) we include a weak coupling between the layers via $-2t_z \cos k_z$ in the dispersion with $t_z \sim 10^{-4}$, which should be present in quasi-two-dimensional organic salts, to provide a consistent bosonic description for the whole phase space.

Naively, we expect that pressure leaves U constant while increasing t, and thus goes as t/U. While J is also affected by pressure as it involves two hopping processes, we chose to study finite temperature phase diagrams with fixed J for simplicity. The $J = 0.25$ phase diagram in Fig. 3(a) shows a strong resemblance to the phase diagram of $EtMe_3P$ found in Refs. [6,22]. Since the VB coverings are completely degenerate, a small anisotropy will break the degeneracy and pick out a single configuration, possibly resulting in the VB ordered phase seen in Ref. [5].

A coupling to the lattice should play an important role in this context as discussed in [6]. Measurement of the spin-lattice relaxation rate, T_1, for the VB ordered state indicates a significant amount of inhomogeneity, possibly due to disorder. Taking this disorder into account could drive the first-order transition we have found theoretically to the second-order transition reported in [6]. Note that near $U \sim 4.2$–4.6 as temperature increases the set of transitions, insulator (dimer) to metal to insulator (SL) occurs, similar to the reentrance seen by resistivity experiments [6].

At lower values of J the SL state persists even at zero temperature, a scenario which has been discussed extensively for the organic compound κ-$(ET)_2Cu_2(CN)_3$ [19,23,24]. The $J = 0$ finite temperature phase diagram is shown in Fig. 3(b) and has a window of SL between a metallic and VB ordered phase, which gets wider at finite temperature due to the larger entropy contained in the SL. It is tempting to argue that at ambient pressure $EtMe_3Sb$ falls into the SL regime with small effective exchange J while $EtMe_3P$ falls belong to the VB ordered phase nearby the SL due to $EtMe_3P$ having a significantly larger value for J. Furthermore, it is possible that $EtMe_3Sb$ itself is close to a dimer instability, but the appearance of definite VB order is suppressed by the β' layer stacking structure [1], and may turn it into a disordered VB state ($\mathbb{Z}_2$ SL) [25]. While thermal transport measurements [3] are consistent with a U(1) SL with a Fermi surface, NMR data at ultralow temperatures [4] suggest spin-gap-like instabilities under a $7.65T$ magnetic field, calling for future study.

As we discussed, the gauge fluctuations are expected to turn the metal-SL transition into a crossover rather than a sharp transition, but the details are still under debate. However, we find that even at the level of mean-field theory, there is difference in the temperature dependence of the specific heat in the SL and metal phases as shown in Fig. 3(c). We note the linear behavior in both metal and insulating phase, with increasing slope as we pass from metal into the SL. This indicates a larger entropy in the insulator, in contrast to conventional MI transition where the density of states decreases to zero, possibly being relevant for paramagnetic phases of $EtMe_3P$ and $EtMe_3Sb$ at finite temperature above the SC and VB states.

It is worthwhile to comment on the absence of magnetic ordering in the phase space considered here. At large U or J one expects magnetic ordering of 120° rotated spins. The magnetic order was considered in [26] where the spin-spin term is decoupled into the χ and magnetic channels, imposing a 120° magnetic ordering. Although they treated the rotor sector differently, at large U/t both methods give the same asymptotic relation $B_{ij} \sim 4t\chi^*_{ij}/U$, which allows us to estimate the critical $U/t \approx 18$, above which the magnetic order sets in for $J/t = 0.25$. Thus our main results near the MI transition are not affected by magnetic ordering of this type. Note that the tendency to order magnetically is also affected by the anisotropy, which distinguishes $EtMe_3P$ and $EtMe_3Sb$ from other $[Pd(dmit)_2]_2$ based organic salts [27].

In summary, we propose an effective model for the isotropic triangular $Pd(dmit)_2$ salts. We show that the Hubbard U and spin exchange interactions account for the diversity present in the phase diagram of the $EtMe_3P$ salt, specifically the proximity of superconductivity and VB order near the pressure induced MI transition. The SL is realized for weak spin-spin interaction, which may be relevant for the $EtMe_3Sb$ salt. Our finite temperature phase diagram shows the reappearance of the SL at finite temperatures due to entropic reasons, explaining the reentrant insulator-metal-insulator transitions reported in $EtMe_3P$. We also present the temperature dependence of the specific heat, which is qualitatively different between the SL and metal and can be tested in future experiments.

We thank A. Paramekanti, M. Hermele, Y. B. Kim, and S. S. Lee for useful discussions. This research was supported by NSERC of Canada and the Canada Research Chair program.

*hykee@physics.utoronto.ca

[1] M. Tamura and R. Kato, Sci. Tech. Adv. Mater. **10**, 024304 (2009).
[2] T. Itou *et al.*, Phys. Rev. B **77**, 104413 (2008).
[3] M. Yamashita *et al.*, Science **328**, 1246 (2010).
[4] S. T. Itou, A. Oyamada, and R. Kato, Nature Phys. **6**, 673 (2010).
[5] M. Tamura *et al.*, J. Phys. Soc. Jpn. **75**, 093701 (2006).
[6] Y. Shimizu *et al.*, Phys. Rev. Lett. **99**, 256403 (2007).
[7] B. J. Powell and R. H. McKenzie, Phys. Rev. Lett. **94**, 047004 (2005).
[8] H. Morita *et al.*, J. Phys. Soc. Jpn. **71**, 2109 (2002).
[9] J. Liu, J. Schmalian, and N. Trivedi, Phys. Rev. Lett. **94**, 127003 (2005).
[10] B. Kyung and A.-M. S. Tremblay, Phys. Rev. Lett. **97**, 046402 (2006).
[11] R. McKenzie and B. Powell, arXiv:1007.5381v1.
[12] L. F. Tocchio *et al.*, Phys. Rev. B **80**, 064419 (2009).
[13] C. Honerkamp, Phys. Rev. B **68**, 104510 (2003).
[14] R. T. Clay, H. Li, and S. Mazumdar, Phys. Rev. Lett. **101**, 166403 (2008).
[15] S. Florens and A. Georges, Phys. Rev. B **66**, 165111 (2002); **70**, 035114 (2004).
[16] B. Braunecker, P. A. Lee, and Z. Wang, Phys. Rev. Lett. **95**, 017004 (2005).
[17] B. J. Powell and R. H. McKenzie, Phys. Rev. Lett. **98**, 027005 (2007).
[18] D. S. Rokhsar, Phys. Rev. B **42**, 2526 (1990).
[19] S.-S. Lee and P. A. Lee, Phys. Rev. Lett. **95**, 036403 (2005).
[20] T. Senthil, Phys. Rev. B **78**, 045109 (2008).
[21] D. Podolsky *et al.*, Phys. Rev. Lett. **102**, 186401 (2009).
[22] T. Itou *et al.*, Phys. Rev. B **79**, 174517 (2009).
[23] Y. Kurosaki *et al.*, Phys. Rev. Lett. **95**, 177001 (2005).
[24] O. I. Motrunich, Phys. Rev. B **72**, 045105 (2005).
[25] M. Levin and T. Senthil, Phys. Rev. B **70**, 220403 (2004).
[26] E. Zhao and A. Paramekanti, Phys. Rev. B **76**, 195101 (2007).
[27] R. Kato *et al.*, J. Am. Chem. Soc. **128**, 10 016 (2006).